8664 Vol. 61, No. 29 / 10 October 2022 / Applied Optics

Research Article

applied optics

On the measurement of remote sensing reflectance by a traditional above-water approach in small water bodies

LIANGFENG CHEN,[1] ZHONGPING LEE,[1,2,*] GONG LIN,[1] YONGCHAO WANG,[1] JUNWEI WANG,[1] AND WENDIAN LAI[1]

[1]State Key Lab of Marine Environmental Science, College of Ocean and Earth Sciences, Xiamen University, Xiamen 361005, China
[2]School for the Environment, University of Massachusetts Boston, Boston, Massachusetts 02125, USA
*Corresponding author: zhongping.lee@umb.edu

Received 1 August 2022; revised 11 September 2022; accepted 20 September 2022; posted 21 September 2022; published 3 October 2022

Small water bodies are an important part of the Earth's freshwater system, protecting biodiversity and providing ecosystem services. Because of various surrounding features, it is unknown to what extent we can obtain accurate remote-sensing reflectance (R_{rs}) of such an environment by the conventional above-water approach (AWA). In this study, we used both AWA and the skylight-blocked approach (SBA) side-by-side to measure R_{rs} in a typical small water body. It was found that the variation of R_{rs} in the UV-blue domain from AWA is around 50% and is inconsistent with the variation of the total absorption coefficient (a_t) obtained from water samples; on the contrary, the variation of R_{rs} obtained from SBA is highly consistent, with a coefficient of variation under ∼5%. These results highlight the large uncertainties in the measured R_{rs} from AWA due to the complexity of such an environment and further echo the robustness of SBA to measure R_{rs} in the field, even in such challenge environments.

https://doi.org/10.1364/AO.472122

1. INTRODUCTION

Small water bodies are the Earth's most abundant and widely distributed freshwater environment. They include ponds, reservoirs, small lakes, rivers, streams, ditches, springs, and other types of water bodies [1–4], which could be natural or man-made, permanent or seasonal [2]. They are fragile and sensitive and are strongly affected by human activities. Static water bodies are easily polluted and difficult to recover, while many naturally formed streams and springs are often reduced due to the exploitation and destruction of mountain forests and soil erosion. These water bodies, although each one could be quite small, are all extremely valuable for the earth's hydrosphere system and human beings. On the one hand, small water bodies can protect the biodiversity of ecosystems that provide the living environment and nutrients needed by aquatic organisms, especially valuable species that are vulnerable to water pollution. Terrestrial animals also often inhabit small water bodies and feed and reproduce there. On the other hand, small water bodies are important to human beings and ecosystems for several reasons: Small water bodies are an important source of water for human life, and also are often used for agricultural irrigation, aquaculture, and leisure activities. Furthermore, small water bodies can promote water circulation in nature, and increase the air humidity in the surrounding areas. Therefore, timely and effective monitoring and protection of the Earth's small water bodies is critically important [1,5].

The traditional method to monitor small water bodies is by collecting water samples from targeted areas and measuring the samples in a laboratory. Such an approach provides discrete measurements, which may not represent the water body as a whole. It is time-consuming to cover the wide range of ponds, reservoirs, and small lakes that exist around the world. Many studies [6,7] have shown that some water-quality indicators, such as water clarity and the concentration of chlorophyll, are directly or indirectly related to the water color, which is commonly represented as the spectrum of water-leaving radiance. Thus, as demonstrated in many studies (e.g., Kupssinskü *et al.* [8], Kim and Choi [9], and Nguyen *et al.* [10]), remote sensing techniques using water color measurement offer the possibility to cover large areas with high temporal and spatial resolution [11]. For such remote sensing approaches, the studies by Kupssinskü *et al.* [8] and Nguyen *et al.* [10]), for example, used matched-up satellite images and *in situ* data to train empirical algorithms. These algorithms (either simple mathematic regressions or machine learning), however, would be image specific and not necessarily applicable to new images or new areas. A more common approach taken by the community of ocean (water) color remote sensing is to separate the data processing of satellite remote sensing into two linked segments: one segment focusing on the generation of remote sensing reflectance (R_{rs}, sr^{-1}) through atmospheric correction [12], and the other focusing on the retrieval of water-quality parameters from R_{rs} through the development of in-water algorithms. After the two steps are mature, they can then be applied to new images and new areas to generate water-quality products from satellite images. It is thus clear that the accurate measurement of R_{rs} in the field is not only important for the validation of atmosphere correction, but also critical for the development of algorithms for water-quality retrieval.

Remote sensing reflectance is defined as the ratio of the water-leaving radiance (L_w) to down-welling irradiance just above the surface ($E_d(0^+)$), where the above-water approach (AWA), in-water approach [IWA], and the skylight-blocked approach (or the on-water approach) have been developed in the past decades [13]. Traditionally, because of the shallow bottom of the lakes and/or reservoirs that limit an adequate application of the IWA [14], the AWA [15] is more commonly adopted to measure R_{rs} in such water bodies, where generally satisfactory results have been reported for large lakes [16]. However, the applicability of the traditional AWA in the environment of small water bodies demands further evaluation. This is because, unlike the open ocean or large lakes, small water bodies are usually surrounded by objects above the ground, such as trees or buildings; consequently, the diffuse reflection of the roughened water surface causes uncertainties in the measured water-leaving radiance (and then R_{rs}). For this reason, we carried out field measurements in the Xiamen University Reservoir to characterize the uncertainties in the measurement of R_{rs} by the traditional AWA in small water bodies. For comparison, R_{rs} was also measured by the SBA at the same time [17,18]. In addition, the absorption coefficients of the water samples were measured as an independent source to verify the observed R_{rs} of this water body. We believe the results of this effort provide guidance for future measurement of remote sensing reflectance in such challenging aquatic environments.

2. METHODS AND SETUPS

A. Study Area

For this study, we selected the Xiamen University Reservoir, which is a typical small water body environment. This reservoir is a closed inland freshwater pond located at the Siming Campus of Xiamen University, Xiamen, Fujian Province, with a surface area of approximately 30,000 m^2 and a water depth of $\sim 1-10$ m. The water is highly eutrophic with a chlorophyll concentration generally higher than 20.0 mg/m^3, and it is generally a deep green color. A more obvious feature of such a small water body environment is that it is surrounded by trees on the mountains, as shown in Fig. 1, which causes various shadows on the surface by blocking light from the sun or sky.

B. Instrument

To facilitate measurements by both AWA and SBA in this water body, we used a spectroradiometer (SE SR1901, Spectral Evolution, Haverhill, MA, USA), which covers wavelengths from 280 to 1900 nm with a spectral resolution of $\sim$2 nm, to collect the relevant radiance. The spectroradiometer was

Fig. 1. Study area of Xiamen University reservoir, a typical small water body environment.

equipped with two sensors: one for radiance and the other with a cosine collector for downwelling irradiance. In this study, we used only the radiance sensor to avoid possible mismatches in radiometric and spectral calibrations between the two sensors, and the downwelling irradiance was obtained through the measurement of radiance reflected from a standard gray card.

Follow the concept of SBA [18], we attached a small black tube in front of the radiance sensor as a shading cone to directly measure the water-leaving radiance. The size of this cone is 19 mm in diameter and 40 mm in length, with an opening wider than the field of view of the radiometer; thus, there was no interference to the radiance measurements. Laboratory tests indicated that the obtained radiance with and without the cone are consistent, thus meeting the requirements of this study.

C. Measurement

We carried out the field measurements in the reservoir on Jan. 9, 2022, under a blue sky with no clouds. The water surface was roughened by wind, as shown in Fig. 1, with a wind speed in the range of 1.2–4.5 m/s during this field experiment. Five locations in the reservoir that were distances apart were selected as the measurement sites, where shadow from the sun was avoided. During these measurements, all precautions were taken to avoid sun shadow and sun glint because it will cause large uncertainties in the measurement of R_{rs}. At every site, all radiometric measurements were completed within $\sim$2 min to minimize the impact of changing solar elevation, and all measurements were carried out by the operators on land, rather than on a vessel.

1. Water-Leaving Radiance by AWA

As described in the ocean optics protocol [19], it is necessary to measure two quantities for the determination of L_w by AWA. The two quantities are: total upwelling radiance above the surface (L_t) and downwelling sky radiance (L_{sky}) from the reciprocal angle of L_t. At each site, we first measured L_t by AWA with a nadir observation angle of 40°, where the radiometer was kept

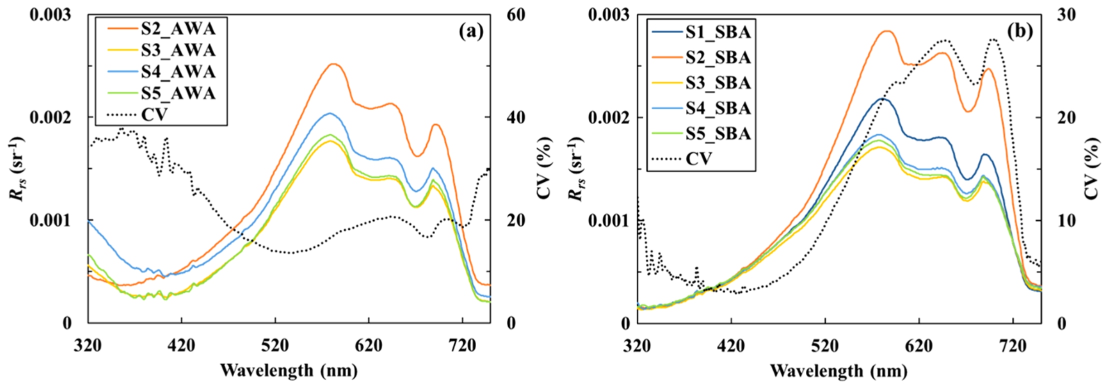

Fig. 2. Spectra of $R_{rs}(\lambda)$ along with their coefficient of variation (CV) of this study: (a) obtained via AWA and (b) obtained via SBA.

~30 cm above the water surface. Although it is recommended to take an azimuth angle of 135° from the sun for measurements by AWA [20], we took an angle around 90° to avoid interference from the shoreline. The L_{sky} was subsequently measured by flipping the sensor toward the sky after completing the collection of L_t. For these measurements, a long black rod of ~1.2 m long was used, as shown in Fig. 1, to extend the measurement of L_t away from the shoreline to minimize the impact of shore features. Both L_t and L_{sky} were measured five times for each site, and the average of each property was used for the data analysis.

Following Mobley [20], L_w can be calculated from the measured L_t and L_{sky} by

$$L_w(\lambda) = L_t(\lambda) - \rho * L_{sky}(\lambda). \quad \textbf{(1)}$$

Here, ρ is the effective surface reflectance that accounts for reflected sky light from all directions for the given sensor direction, and a value of 0.025 was taken for this study; in general, however, ρ is a function of wavelength when the relationship among L_w, L_t, and L_{sky} is mathematically modeled as Eq. (1) [21].

2. Water-Leaving Radiance by SBA

After completing the measurements of L_t and L_{sky} at each site, the cone was attached in front of the radiometer with the opening end of the cone inserted right below the surface; thus, L_w was measured directly following SBA. The SBA processing to get R_{rs} followed what was described in the literature [22,23]. In short, we used the average (μ) and standard deviation (σ) of the median radiance in the 750–800 nm range to filter out likely error scans. The threshold is $\mu + 3\sigma$ [17], and data that exceed this standard were excluded. Due to the strictly controlled environment and settings, only about 3% of the original data were excluded in the subsequent analysis of this study. The self-shading effect was corrected following Yu *et al*. [24].

R_{rs} is defined as the ratio of L_w to downwelling irradiance just above the surface (E_d). In this study, radiance (L_{gc}) reflected from the standard gray card was measured to determine E_d, which was calculated as

$$E_d(\lambda) = \frac{\pi * L_{gc}(\lambda)}{R_{gc}}, \quad \textbf{(2)}$$

with R_{gc} (= 0.2) the reflectance of the gray card. The same E_d was applied to L_w from both AWA and SBA for the calculation of R_{rs} from the two schemes.

3. Measurements of Inherent Optical Properties

We also collected water samples from the surface at each site to measure their inherent optical properties (IOPs) in the lab, which include the absorption coefficients of gelbstoff (a_g) and particles (a_p). The instrument for such measurements is a dual-beam PE Lambda 950 spectrophotometer equipped with an integrating sphere that is 150 mm in diameter. The spectrum of a_p was measured with the transmittance–reflectance (T–R) method [25] after the water sample was filtered by GF/F filters for 30 ml following the filter-pad technique [26] and a_g was measured following Bricaud *et al*. [27]. With the measured a_g and a_p, the total absorption (a_t) of each station was calculated as the sum of the pure-water absorption coefficient (a_w), a_g, and a_p, with values of a_w taken from Mason *et al.* [28], where its slight dependence on temperature [29,30] was ignored.

3. RESULTS AND DISCUSSION

A. Comparison of R_{rs} Spectra

Figure 2 shows the resulted R_{rs} spectra; Fig. 2(a) shows the spectra from AWA and Fig. 2(b) shows the spectra from SBA. The comparison is limited to wavelengths in the 320–750 nm

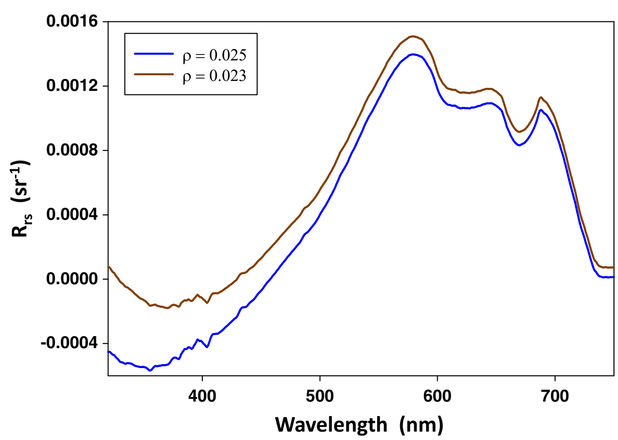

Fig. 3. $R_{rs}(\lambda)$ spectrum via AWA for Station 1 of this study.

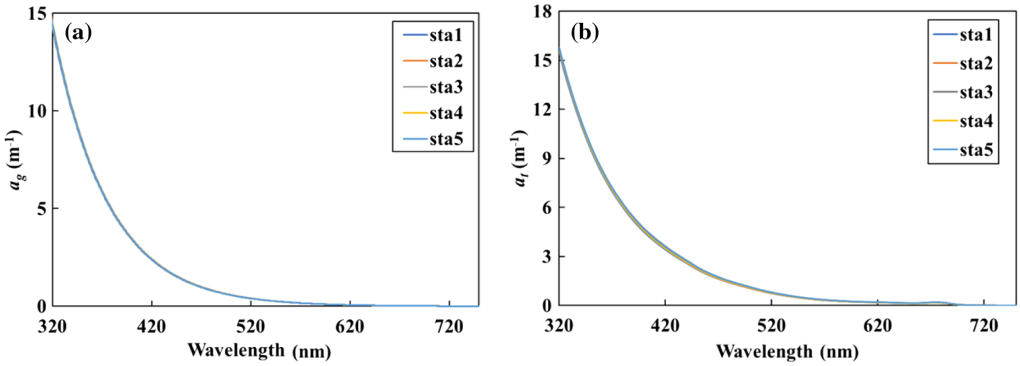

Fig. 4. Spectra of (a) a_g and (b) a_t obtained during this study.

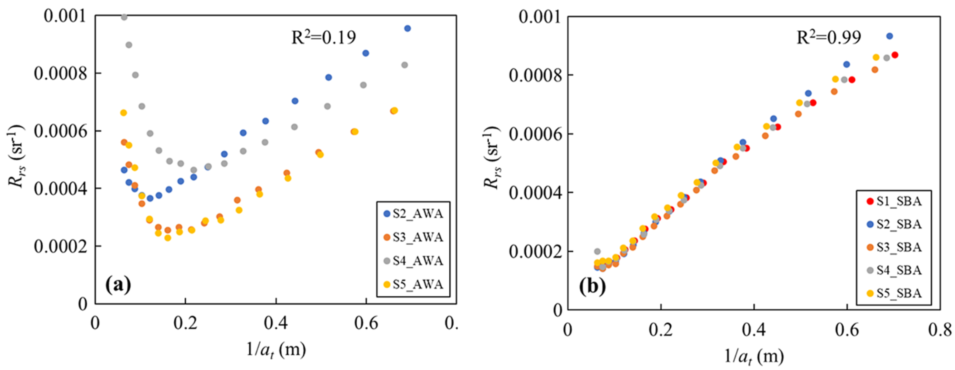

Fig. 5. Scatterplots between $1/a_t$ and R_{rs} for wavelengths in the range of 320–480 nm (every 10 nm): (a) for R_{rs} measured by AWA and (b) for R_{rs} measured by SBA.

range because the self-shading correction was only applied to this spectral range. Overall, the spectral characteristics of R_{rs} spectra obtained by AWA and SBA are consistent, where the R_{rs} values are very small in the UV-blue domain, with an R_{rs} peak around 570 nm, and a second R_{rs} peak around 700 nm. At the same time, the highest R_{rs} values are less than ~0.003 sr^{-1}. These features in R_{rs} spectra reflect the dominance of absorption by colored dissolved organic matter (CDOM, presented later), while there are insignificant suspended sediments for waters in such a reservoir. Note that R_{rs} from just four of the five stations by AWA are included in Fig. 2(a), while R_{rs} from SBA included all five stations in Fig. 2(b). This is because the R_{rs} spectra of Sta. 1 measured via AWA show negative R_{rs} values for wavelengths in the blue, even if a smaller ρ value was used, as shown in Fig. 3. This result echoes the strong dependence of reliable R_{rs} from AWA on accurate measurement L_{sky} and accurate determination of ρ for wind-roughened surface [20,21].

Because of the change in the bottom depths and bottom reflectance, R_{rs} spectra from both AWA and SBA show visible variations in the ~520−720 nm range. Note that the R_{rs} spectra from AWA and SBA unfortunately were not measured simultaneously, but it does not affect the conclusions of this study. What is striking between the two groups of R_{rs} spectra is the contrast of R_{rs} for the wavelengths of the ~320−480 nm range. With an increase in the wavelength, R_{rs} values from AWA generally decreased from 320 nm to ~400 nm and then increased, and there are large deviations [around 30%, as shown by the black-dot line in Fig. 2(a)] of R_{rs} values among the five stations, including the nonrealistic R_{rs} of Sta. 1 shown in Fig. 3. However, for the same wavelength range, R_{rs} values from SBA generally increased from 320 nm to ~480 nm, and the deviation among the five stations was less than ~5%, as shown by the black-dot line in Fig. 2(b). The increase in the AWA-obtained R_{rs} with a decrease in the wavelength for the 400–320 nm range indicates insufficient correction of the reflected sky radiance [21].

To verify this significant contrast, we compared the measured a_g and a_t spectra of the five stations (see Fig. 4), which shows that for such a small reservoir, the a_t spectra are quite spatially uniform, with gelbstoff of the dominate player in the UV-blue domain [$a_g(350)$ as high as ~8.0 m^{-1}, as shown in Fig. 4)]. Considering that R_{rs} is an inverse function of a_t [31,32] and that a_t are nearly uniform, as shown in Fig. 4, the spectral curvature and the variation of $R_{rs}(320-480)$ obtained by AWA are not supported by the data of $a_t(320-480)$, but $R_{rs}(320-480)$ obtained by SBA are highly consistent with

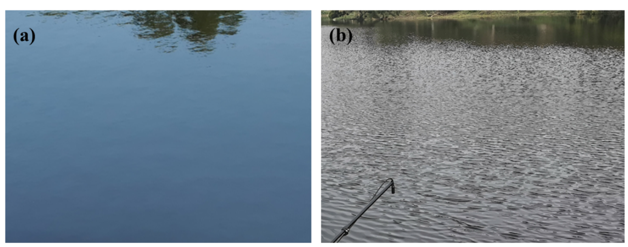

Fig. 6. Water surface under different wind speed at Station 3: (a) 1.2 m/s and (b) 3.5 m/s.

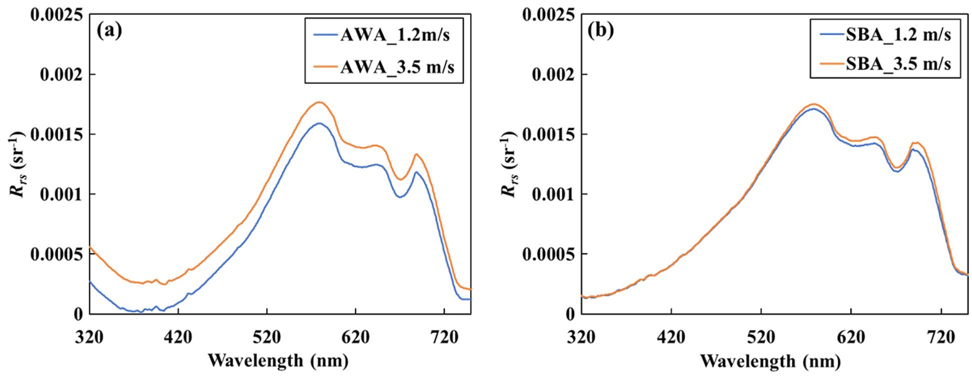

Fig. 7. R_{rs} spectra obtained under different wind speed at Station 3: (a) obtained R_{rs} via AWA and (b) obtained R_{rs} via SBA.

that of $a_t(320-480)$. This is further echoed by the relationships presented in Fig. 5, which shows scatterplots between $R_{rs}(320-480)$ and $a_t(320-480)$, for R_{rs} from AWA and SBA, respectively, with a wavelength interval of 10 nm. There are no clear relationships [coefficient of determination $(R^2) = 0.19$] between $1/a_t(320-480)$ and AWA's $R_{rs}(320-480)$, but the R^2 value is 0.99 between $1/a_t(320-480)$ and SBA's $R_{rs}(320-480)$, supporting the modeling results from the radiative transfer equation [31,32]. These results further indicate that SBA is a robust approach to measure R_{rs} in such a complex environment.

B. Factors Affecting AWA R_{rs} in Small Water Bodies

For the determination of R_{rs} by AWA, the biggest challenge is the removal of surface reflected radiance [21], where L_{sky} from the reciprocal angle of L_t is measured and used in the data processing (see Eq. 1). However, for roughened sea (water) surface, the reflected light comes from a large portion of the sky (see Fig. 1 of Mobley [20]); thus, it is challenging to determine the L_{sky} from which direction best representing the incoming source of reflected light [21]. This becomes even worse for small water bodies due to the surrounding trees or buildings. During our experiment, we encountered a sudden change of wind speed, so the next section discusses the uncertainties introduced by these environmental factors when R_{rs} is measured by AWA, while at the same time highlighting that SBA is immune to such factors.

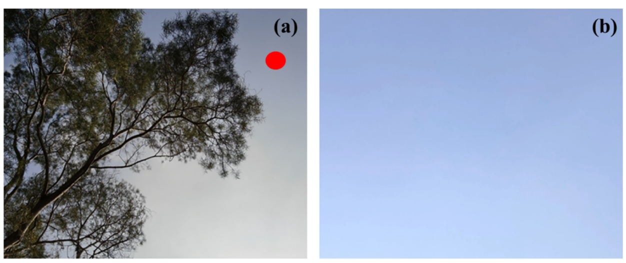

Fig. 8. (a) Picture of sky near treetops. The red dot represents the direction that the spectrometer was pointing for the measurement of L_{sky}. (b) Picture of blue sky.

1. *Change of Wind Speed*

During the measurement at Sta. 3, the wind speed was ~1.2 m/s, which was changed to 3.5 m/s ~ 30 min later; thus, the surface was significantly roughened, as shown in Fig. 6. We took both AWA and SBA measurements again for this site, with the resulting R_{rs} from both schemes (under two wind speeds) shown in Fig. 7. For the same water body, the R_{rs} from AWA under two different wind speeds showed an obvious difference for the entire spectrum, and the relative difference is more than 100% in the UV-blue domain. As indicated by Eq. (1), this difference is subject to the value of ρ to be applied. Note that for such a shallow bottom reservoir, the surface wind slope does not follow what Cox and Munk predicted [33]; thus, a selection of the proper ρ value for such inland water bodies is a challenge. However, the R_{rs} from SBA under the two different wind speeds is nearly identical, especially in the UV-blue domain. The highest difference (at ~570 nm) is around 7%, which is likely due

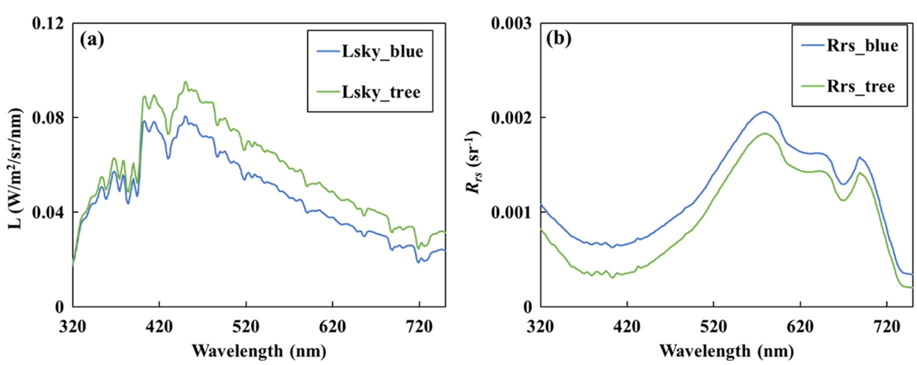

Fig. 9. (a) L_{sky} measured near treetops and from blue sky. (b) R_{rs} of the same location obtained from two different azimuth angles.

to slightly different positions for the two measurements. This consistency in R_{rs} further highlights the robustness of SBA for the measurement of R_{rs} in the field.

2. Sky Radiance

For AWA, as discussed earlier, one of the biggest challenges is to determine the representative L_{sky} that can be applied to Eq. (1) to calculate L_w. This is even more challenging for small water bodies because the surrounding trees or objects further complicate the radiance reflected by surface and collected by the radiometer when it measures L_t. Figure 8 shows two pictures: Fig. 8(a) has treetops in the direction (the red spot) of measuring L_{sky}, and Fig. 8(b) has a completely open sky in the direction of measuring L_{sky}; i.e., L_{sky} obtained from two different azimuth angles and shown in Fig. 9(a). For the same location with two different orientations for both L_t and L_{sky}, the resulted R_{rs} are presented in Fig. 9(b), where the difference in R_{rs} is as high as ~50% for wavelengths around 410 nm, which further highlights the difficulty to obtain accurate R_{rs} by AWA in such environments. However, because the R_{rs} measurement by SBA does not require the measurement of L_{sky}, a much more accurate and reliable determination of R_{rs} can be obtained from SBA, as shown in Fig. 2, for such challenging environments.

4. CONCLUSION

In this study, R_{rs} was measured by both AWA and SBA in the reservoir of Xiamen University, which is a typical small water body. The results indicate that the surrounding trees and other features above the ground further amplify the difficulty to reasonably remove the surface-reflected light by the wind-roughened water surface, and then to obtain reliable R_{rs} with the traditional AWA. On the other hand, the R_{rs} spectra obtained by SBA are highly supported by the absorption data from the water samples. These results show that SBA is not only a robust approach to measure L_w (and then R_{rs}) in the ocean and marine environments, it is even better for complex small water bodies.

Funding. National Natural Science Foundation of China (41830102, 41890803, 41941008).

Acknowledgment. The authors greatly appreciate the support from the National Natural Science Foundation of China and Xiamen University and the constructive comments and suggestions from two anonymous reviewers.

Disclosures. The authors declare that they have no known competing financial interests or personal relationships that could have appeared to influence the work reported in this paper.

Data availability. Data used in this study may be obtained from the authors upon request.

REFERENCES

1. J. Biggs, S. von Fumetti, and M. Kelly-Quinn, "The importance of small waterbodies for biodiversity and ecosystem services: implications for policy makers," Hydrobiologia **793**, 3–39 (2016).
2. L. Hu, D. He, and H. Shi, "Microplastics in inland small waterbodies," in *Microplastics in Terrestrial Environments* (2020), pp. 93–110.
3. R. M. Igamberdiev, G. Grenzdoerffer, R. Bill, H. Schubert, M. Bachmann, and B. Lennartz, "Determination of chlorophyll content of small water bodies (kettle holes) using hyperspectral airborne data," Int. J. Appl. Earth Obs. Geoinf. **13**, 912–921 (2011).
4. W. D. Riley, E. C. Potter, J. Biggs, *et al.*, "Small water bodies in Great Britain and Ireland: Ecosystem function, human-generated degradation, and options for restorative action," Sci. Total Environ. **645**, 1598–1616 (2018).
5. R. M. Igamberdiev, B. Lennartz, G. Grensdoerffer, R. Bill, and H. Schubert, "Analysis of spectral signatures of small water bodies (kettle holes) in the agricultural young moraine landscape of north-eastern Germany," Int. J. Remote Sens. **31**, 5495–5511 (2010).
6. U. Turdukulov and Z. Vekerdy, "Determination of water quality parameters using imaging spectrometry (case study for Sajó flood plain, Hungary)," in *Proceedings of the Earsel Workshop on Imaging Spectrometry, F* (2003).
7. S. Sathyendranath, ed., "Remote sensing of ocean colour in coastal, and other optically-complex, waters," in Reports of the International Ocean-Colour Coordinating Group (IOCCG) (2000), p. 140.
8. L. S. Kupssinskü, T. T. Guimarães, E. Menezes de Souza, D. C. Zanotta, M. R. Veronez, L. Gonzaga, Jr, and F. F. Mauad, "A method for chlorophyll-a and suspended solids prediction through remote sensing and machine learning," Sensors **20**, 2125 (2020).
9. H. Kim and Y. Choi, "Location estimation of autonomous driving robot and 3D tunnel mapping in underground mines using pattern matched LiDAR sequential images," Int. J. Min. Sci. Technol. **31**, 779–788 (2021).
10. N. B. Nguyen, M.-K. Kim, Q. T. Le, D. N. Ngo, K.-D. Zoh, and S.-W. Joo, "Spectroscopic analysis of microplastic contaminants in an urban wastewater treatment plant from Seoul, South Korea," Chemosphere **263**, 127812 (2021).
11. C. B. Mouw, S. Greb, D. Aurin, P. M. DiGiacomo, Z. Lee, M. Twardowski, C. Binding, C. Hu, R. Ma, and T. Moore, "Aquatic color radiometry remote sensing of coastal and inland waters: Challenges and recommendations for future satellite missions," Remote Sens. Environ. **160**, 15–30 (2015).
12. M. Wang, "Atmospheric correction for remotely-sensed ocean-colour products," in Reports and Monographs of the International Ocean-Colour Coordinating Group (IOCCG) (2010).
13. K. G. Ruddick, K. Voss, E. Boss, A. Castagna, R. Frouin, A. Gilerson, M. Hieronymi, B. C. Johnson, J. Kuusk, and Z. Lee, "A review of protocols for fiducial reference measurements of water-leaving radiance for validation of satellite remote-sensing data over water," Remote Sens. **11**, 2198 (2019).
14. R. C. Smith, C. R. Booth, and J. L. Star, "Oceanographic biooptical profiling system," Appl. Opt. **23**, 2791–2797 (1984).
15. J. L. Mueller, C. Davis, R. Arnone, R. Frouin, K. Carder, Z. Lee, R. Steward, S. Hooker, C. D. Mobley, and S. McLean, "Above-water radiance and remote sensing reflectance measurements and analysis protocols," in *Ocean Optics Protocols for Satellite Ocean Color Sensor Validation Revision* (2000), Vol. **2**, pp. 98–107.
16. B. Zhang, J. Li, Q. Shen, and D. Chen, "A bio-optical model based method of estimating total suspended matter of Lake Taihu from near-infrared remote sensing reflectance," Environ. Monit. Assess. **145**, 339–347 (2008).
17. Z. P. Lee, N. Pahlevan, Y.-H. Ahn, S. Greb, and D. O'Donnell, "Robust approach to directly measuring water-leaving radiance in the field," Appl. Opt. **52**, 1693–1701 (2013).
18. Y. Ahn, J. Ryu, and J. Moon, "Development of redtide & water turbidity algorithms using ocean color satellite," KORDI Report No BSPE 98721-00 (1999).
19. J. L. Mueller and R. W. Austin, "Ocean optics protocols for SeaWiFS validation, revision 1," Oceanogr. Lit. Rev. **9**, 805 (1995).
20. C. D. Mobley, "Estimation of the remote-sensing reflectance from above-surface measurements," Appl. Opt. **38**, 7442–7455 (1999).
21. Z. P. Lee, Y. H. Ahn, C. Mobley, and R. Arnone, "Removal of surface-reflected light for the measurement of remote-sensing reflectance from an above-surface platform," Opt. Express **18**, 26313–26324 (2010).
22. J. Wei, M. Wang, Z. Lee, M. Ondrusek, S. Zhang, and S. Ladner, "Experimental analysis of the measurement precision of spectral water-leaving radiance in different water types," Opt. Express **29**, 2780–2797 (2021).
23. Z. Shang, Z. Lee, Q. Dong, and J. Wei, "Self-shading associated with a skylight-blocked approach system for the measurement of

water-leaving radiance and its correction," Appl. Opt. **56**, 7033–7040 (2017).
24. X. L. Yu, Z. P. Lee, Z. H. Shang, H. Lin, and G. Lin, "A simple and robust shade correction scheme for remote sensing reflectance obtained by the skylight-blocked approach," Opt. Express **29**, 470–486 (2021).
25. S. Tassan and G. M. Ferrari, "Variability of light absorption by aquatic particles in the near-infrared spectral region," Appl. Opt. **42**, 4802–4810 (2003).
26. D. A. Kiefer and J. B. SooHoo, "Spectral absorption by marine particles of coastal waters of Baja California 1," Limnol. Oceanogr. **27**, 492–499 (1982).
27. A. Bricaud, A. Morel, and L. Prieur, "Absorption by dissolved organic matter of the sea (yellow substance) in the UV and visible domains," Limnol. Oceanogr. **26**, 43–53 (1981).
28. J. D. Mason, M. T. Cone, and E. S. Fry, "Ultraviolet (250–550 nm) absorption spectrum of pure water," Appl. Opt. **55**, 7163–7172 (2016).
29. R. Röttgers, D. McKee, and C. Utschig, "Temperature and salinity correction coefficients for light absorption by water in the visible to infrared spectral region," Opt. Express **22**, 25093–25108 (2014).
30. G. Wei, Z. Lee, X. Wu, X. Yu, S. Shang, and R. Letelier, "Impact of temperature on absorption coefficient of pure seawater in the blue wavelengths inferred from satellite and in situ measurements," J. Remote Sens. **2021**, 9842702 (2021).
31. H. R. Gordon, O. B. Brown, R. H. Evans, J. W. Brown, R. C. Smith, K. S. Baker, and D. K. Clark, "A semianalytic radiance model of ocean color," J. Geophys. Res. **93**, 10909–10924 (1988).
32. Z. Lee, K. L. Carder, and K. Du, "Effects of molecular and particle scatterings on the model parameter for remote-sensing reflectance," Appl. Opt. **43**, 4957–4964 (2004).
33. C. Cox and W. Munk, "Measurement of the roughness of the sea surface from photographs of the sun's glitter," J. Opt. Soc. Am. **44**, 838–850 (1954).